Stability and Kinetics of Nucleic Acid Triplexes with Chimaeric DNA/RNA Third Strands†

Eloy Bernal-Méndez‡ and Christian J. Leumann*

Department of Chemistry & Biochemistry, University of Bern, Freiestrasse 3, CH-3012 Bern, Switzerland

Received April 8, 2002; Revised Manuscript Received August 22, 2002

ABSTRACT: A series of chimaeric DNA/RNA triplex-forming oligonucleotides (TFOs) with identical base sequence but varying sequential composition of the sugar residues were prepared. The structural, kinetic, and thermodynamic properties of triplex formation with their corresponding double-helical DNA target were investigated by spectroscopic methods. Kinetic and thermodynamic data were obtained from analysis of nonequilibrium UV-melting and annealing curves in the range of pH 5.1−6.7 in a 10 mM citrate/phosphate buffer containing 0.1 M NaCl and 1 mM EDTA. It was found that already single substitutions of ribo- for deoxyribonucleotides in the TFOs greatly affect stability and kinetics of triplex formation in a strongly sequence dependent manner. Within the sequence context investigated, triplex stability was found to increase when deoxyribonucleotides were present at the 5′-side and ribonucleotides in the center of the TFO. Especially the substitution of thymidines for uridines in the TFO was found to accelerate both the association and dissociation process in a strongly position-dependent way. Differential structural information on triplexes and TFO single-strands was obtained from CD-spectroscopy and gel mobility experiments. Only minor changes were observed in the CD spectra of the triplexes at all pH values investigated, and the electrophoretic mobility was nearly identical in all cases, indicating a high degree of structural similarity. In contrast, the single-stranded TFOs showed high structural variability, as determined in the same way. The results are discussed in the context of the design of TFOs for therapeutic or biochemical applications.

Nucleic acids typically occur as right-handed Watson−Crick duplexes of the A- or B-conformational type, or as structurally organized single strands. Besides this, a large number of other structural motifs, e.g., Z-DNA, i-form DNA, G-quartets, or triple helices exist, and attempts were made to assess their biological role. (*1*) The earliest known nonduplex structures are the triple helices that were discovered first for polyribonucleotides (*2*, *3*) and later for polydeoxyribonucleotides and RNA/DNA hybrids (*4*, *5*). Two events within the last couple of decades have triggered the interest in triple-helix chemistry and biology, namely, the discovery of intramolecular triple helices in vivo (H-DNA, *6*) and the possibility of targeting DNA double helices with short triplex forming oligonucleotides (TFOs) (*7*, *8*). The latter finding especially opened the way to a wide variety of potential uses of TFOs, e.g., as therapeutics (antigene strategy) or as tools in molecular biology (*9*−*11* for review).

In the parallel triple-helical binding motif, a homopyrimidine TFO binds to the homopurine strand of double-helical DNA via formation of Hoogsteen hydrogen bonds, so that C^+:G•C and T:A•T base triplets are formed (see ref *12* for review). Both, RNA- and DNA-based TFOs are able to form triple helices with a complementary DNA duplex. Recent studies based on indirect spectroscopic methods have assigned a higher thermal stability to R:D•D triplexes as compared to D:D•D triplexes (*13*−*17*). In contrast, direct, model-independent calorimetric methods indicated similar thermodynamic stabilities for both kinds of triplexes (*18*, *19*). Analyses by NMR spectroscopy have shown that in both D:D•D and R:D•D triple helices, the TFOs display heterogeneous backbone structures, with energetically compromised conformations for certain ribo- and deoxyribonucleotides in the three strands (*14*, *20*−*25*). In particular, protonated (deoxy)cytidines in RNA or DNA TFOs are generally found in N-type conformation (C3′-endo), while uridines and thymidines are found in N-type and S-type conformations, respectively.

Not only the thermodynamic but also the kinetic properties of DNA triple-helix formation are important in the context of the use of TFOs for biological applications, e.g., as competitors for proteins in DNA binding. The scarcely available data show that the rate of triplex formation is 2−3 orders of magnitude slower than that of duplex formation (*26*, *27*). Multivalent cations are known to accelerate the process of triple-helix formation to a larger extent than that for duplex formation, due to the higher charge density of the triplexes (*28*). Differential kinetic data for D:D•D and R:D•D triplex formation are particularly rare. Escudé et al.

† This work was supported by the Swiss National Science Foundation (Grant No. 20-63582.00).

* Corresponding author. Phone: +41 (31) 631-4355. E-mail: leumann@ioc.unibe.ch.

‡ Present address: BioMérieux s.a., Department of Molecular Biology. Chemin de l'Orme 69280-Marcy l'Etoile, France.

[1] Abbreviations: TFO, triplex-forming oligonucleotide; rC, cytidine; rU, uridine; dC, deoxycytidine; dT, thymidine; dU, 2′-deoxyuridine. Hoogsteen-type hydrogen bonds are indicated with ":", and Watson−Crick ones with "•".

10.1021/bi025937m CCC: $22.00
Published on Web 10/08/2002

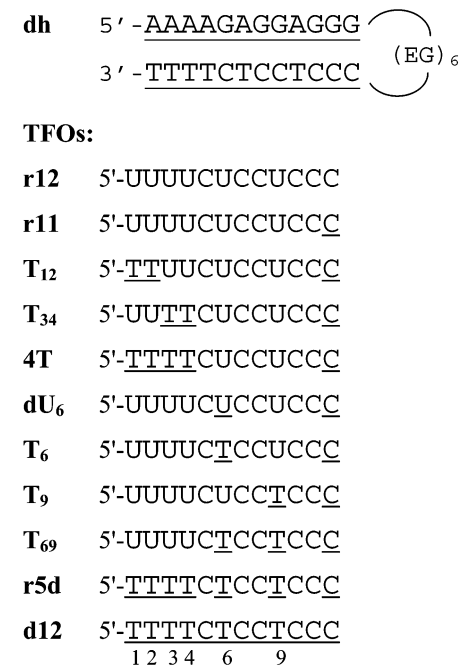

FIGURE 1: Sequence and composition of the oligonucleotides. EG: ethylenglycol linker. Underlined characters indicate deoxyribonucleotides and not underlined characters ribonucleotides.

(*16*) found that the presence of a RNA TFO decreases the rate of triplex formation relative to a DNA TFO, while increasing its stability. Torigoe et al. (*19*), in contrast, find very similar rate constants for the formation of D:D·D and R:D·D triplexes, as well as similar stabilities.

Much effort has been invested in the past to bring thermodynamic stability to DNA duplexes and triplexes via chemical modification of the nucleotide building blocks. However, recent results in our and other laboratories showed thus far no understood differences in affinity as a function of the sequence and the position of the modified nucleotides in the chain (*29*−*31*). To understand such effects in more detail, we recently developed a combinatorial method in which individuals were selected from a TFO library with binding efficiency to their DNA target as the selection criterium. In a first set of experiments, we evaluated the effect of conformational heterogeneity in the backbone on triplex stability, using a library of chimaeric ribo- and deoxyribonucleotide-containing TFOs within a given base regimen (*32*). Here we present a detailed thermodynamic, kinetic, and structural study with individual RNA/DNA TFOs that emerged as interesting candidates from this library (Figure 1).

MATERIALS & METHODS

Oligonucleotides. The TFOs were synthesized, deprotected, and purified as described (*32*). The double helix (**dh**) was synthesized as a hairpin, using an ethyleneglycol-linker (spacer-C18, Glen Research) as the loop element. All oligonucleotides were stored in MilliQ water at −20 °C. The concentration of the samples was calculated from the absorption at 260 nm, using nearest-neighbor approximation for the calculation of the extinction coefficient (*33*). For the formation of the triple helices, 2 nmol of the corresponding strands was mixed, lyophilized to dryness, and dissolved in 1 mL of a 0.1 M NaCl, 1 mM EDTA, 10 mM Citrate/Phosphate buffer (pH 5.1−6.7) to give a final triplex concentration of 2 μM. Annealing was performed by heating the solution to 85 °C for 3 min in a water bath and allowing it to slowly cool to room temperature, and then to 4 °C overnight.

UV-Melting Experiments. The experiments were performed on a Cary-3E UV−vis spectrophotometer (Varian), using a heating−cooling−heating cycle between 0 and 90 °C, with a 8.3×10^{-3} K/s linear gradient. The absorption was measured every 1 °C at 260 and 300 nm. Data were analyzed using Origin50 software. For the triplex to duplex transition, the heating and cooling profiles of the melting curves were not superimposable. The maximum melting temperatures (T_{max}) were defined as the melting temperatures of the heating (in contrast to cooling) curve. Heating and cooling profiles of the duplex to coil transition were always superimposable.

Determination of Kinetic Data from UV-Melting Curves. The observed hysteresis in melting and annealing curves depends on the temperature of the transition, the heating or cooling rate, the pH, the nature of the third strand, and the triplex concentration. This allowed us to determine the association (k_{on}) and dissociation (k_{off}) rate constants as a function of the temperature from the melting curves (λ = 260 nm), applying the mathematical model described by Rougée et al. (*28*). Using a two-state model, the equilibrium for the triplex to duplex transition can be written as

$$\mathrm{TFO} + \mathrm{dh} \underset{k_{off}}{\overset{k_{on}}{\rightleftharpoons}} \mathrm{th}$$

where dh stands for double helix and th for the triple helix, with the rate equation being

$$\mathrm{d[th]}/\mathrm{d}t = k_{on}[\mathrm{TFO}][\mathrm{dh}] - k_{off}[\mathrm{th}] \qquad (1)$$

From the normalized experimental absorbance versus temperature curve (α-curve), the association factor α (α = 1 for complete hybridization, α = 0 for complete dissociation) can be obtained for both the heating and the cooling curves. The use of α in the rate eq 1 directly gives

$$\mathrm{d}(\alpha_c)/\mathrm{d}t = k_{on}c(1-\alpha_c)^2 - k_{off}(\alpha_c) \qquad (2a)$$

$$\mathrm{d}(\alpha_h)/\mathrm{d}t = k_{on}c(1-\alpha_h)^2 - k_{off}(\alpha_h) \qquad (2b)$$

where α_c and α_h are the association factors for the heating and cooling profile, respectively, and c is the molar concentration of the TFO and dh ($= 2 \times 10^{-6}$ M, equal stoichiometric ratio of dh and TFO). Substitution of the cooling and heating rates ($\mathrm{d}T/\mathrm{d}t$) that are known into eqs 2a and 2b yield two linear equations with the two variables k_{on} and k_{off}

$$\mathrm{d}(\alpha_c)/\mathrm{d}T = (\mathrm{d}T/\mathrm{d}t)^{-1}[k_{on}c(1-\alpha_c)^2 - k_{off}(\alpha_c)] \quad (3a)$$

$$\mathrm{d}(\alpha_h)/\mathrm{d}T = -(\mathrm{d}T/\mathrm{d}t)^{-1}[k_{on}c(1-\alpha_h)^2 - k_{off}(\alpha_h)] \quad (3b)$$

From this, the rates of association and dissociation can be determined. The activation energies for the association and dissociation (E_{on} and E_{off}), as well as the thermodynamic melting temperature (T_m, defined as T at α = 0.5), can then

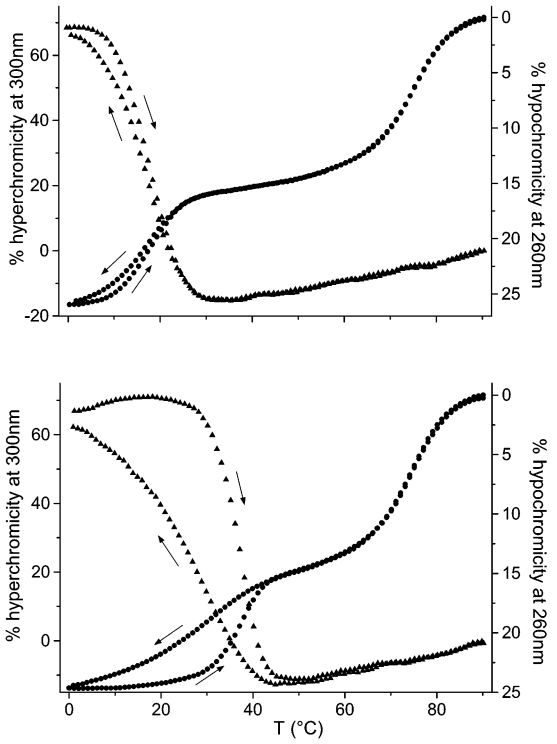

FIGURE 2: Typical UV-thermal profiles (pH 5.9) obtained for **d12:dh** (top) and **r12:dh** (bottom) at 260 nm (●) and 300 nm (▲). The arrows indicate the direction of the temperature gradient.

be determined using the modified Arrhenius equations

$$\ln(c\cdot k_{on}/2) = -E_{on}/(RT) + \ln(c/2) \quad (4a)$$

$$\ln(k_{off}) = -E_{off}/(RT) \quad (4b)$$

from the slopes and the intersection point of the plot of $\ln(c\cdot k_{on}/2)$ and $\ln(k_{off})$, as a function of $1/T$ (see Figure 3).

Circular Dichroism. CD measurements were performed using a Jasco J715 spectropolarimeter coupled to a Jasco PFD-350S peltier temperature controller. Samples were prepared as indicated for the UV melting experiments. Spectra were recorded at 5°C, between 210 and 320 nm, at 0.5 nm steps. Each spectrum represents the average of six measurements. Data were analyzed using Origin50 software.

Gel Shift Assay. TFOs or dh were radiolabeled at the 5′-side with T4 polynucleotide kinase (APBiotech) and γ-^{32}P-ATP (Hartmann) according to standard protocols. Triplex (12μM, 10 μL) or TFO (12μM, 10 μL) in 100 mM NaOAc, 1 mM EDTA, pH 5.5, was heated to 60°C for 3 min and then cooled to 4°C and left overnight. Three microliters of each sample was then mixed with 1 μL 40% glucose and charged on a nondenaturing, 20% polyacrylamide gel using a 0.1 M sodium acetate, 1 mM EDTA solution at pH 5.5 as running buffer. The electrophoresis was performed at 250 V, for 25 h at 4°C. The results were visualized and processed on a Molecular Dynamics PhosphorImager using ImageQuant software (version 3.3).

RESULTS

Figure 1 summarizes the double-helical DNA target and the TFOs used in this study. The TFOs were found previously to show distinct differences in affinity to their target,

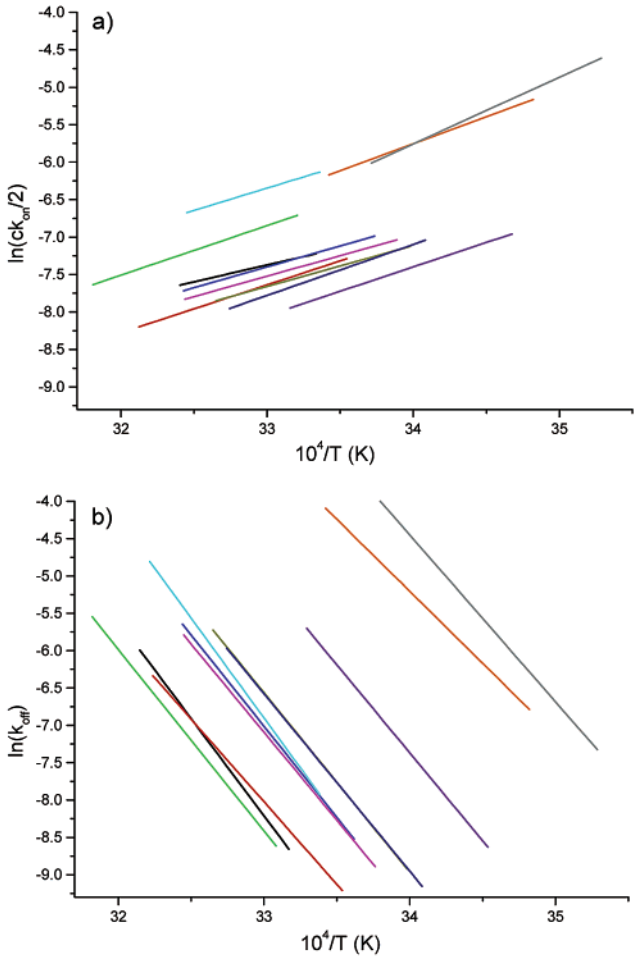

FIGURE 3: Linear plots of $\ln(c\cdot k_{on}/2)$ (a) $\ln(k_{off})$ (b) vs T^{-1} for each triplex as obtained from UV-annealing and melting curves according to the mathematical treatment outlined in the materials and methods section. The plots are linear regression fits based on 10−15 experimental values per plot with $r > 0.990$ for plots in panel a and >0.998 for the plots in panel b. Conditions: 0.1 M NaCl, 1 mM EDTA, 10 mM citrate/phosphate buffer, pH 5.9. 2 μM th. Black, **r12**; red, **r11**; green, $\mathbf{T_{12}}$; blue, $\mathbf{T_{34}}$; cyan, **4T**; magenta, $\mathbf{dU_6}$; dark yellow, $\mathbf{T_6}$; dark blue, $\mathbf{T_9}$; purple, $\mathbf{T_{69}}$; orange, **r5d**; gray, **d12**.

depending on the number, the nature, and the position of the ribo- or deoxyribonucleotide units (*32*). The triple helices formed are pH-dependent, since the cytosines in the third strand have to be protonated in order to form two hydrogen bonds with guanines. Thus, control of the pH in the range of 5.0−7.0 allows for a tuning of the triplex stability without perturbing duplex stability.

The formation of a double helix from two single strands or from a random-coiled hairpin produces a hypochromic effect at the UV absorption of the nucleotides in the wavelength range of 240−290 nm. This effect can be followed by measuring the absorption of the sample at a fixed wavelength within this range as a function of the temperature. A wavelength of 260 nm, near to the maximum of the absorption band of the nucleobases, is commonly used. Likewise, the formation of a triple helix from a duplex and a pyrimidine-rich single strand is also associated with a hypochromic effect at 260 nm, so that this process can be followed in the same way as for the double helix. In addition, a hyperchromic effect at around 300 nm occurs upon triplex formation, most likely due to cytosine partial protonation (*34*). This effect is absent in the case of double helix melting.

Table 1: Thermodynamic and Kinetic Data (pH 5.9, 30°C) of Triple-Helix Formation as Determined from the Heating and Cooling Profiles of the UV-Melting Curves (see materials and methods section)[a]

TFO	T_m[b]	T_{max}[b]	k_{on}[c]	k_{off}[d]	E_{on}[e,f]	E_{off}[e,g]
r12	32.4	37.7	789.4	6.63×10^{-5}	−8.9	51.6
r11	31.2	37.8	669.9	9.91×10^{-5}	−12.7	43.8
T_{12}	34.6	39.2	1493.9	5.96×10^{-5}	−13.1	48.1
T_{34}	28.6	33.4	815.6	24.03×10^{-5}	−11.0	48.4
4T	31.5	34.0	2383.9	23.71×10^{-5}	−11.8	52.9
dU_6	28.7	33.8	715.8	23.24×10^{-5}	−10.8	46.7
T_6	26.5	32.3	623.9	38.53×10^{-5}	−10.8	47.5
T_9	26.3	31.7	594.7	38.53×10^{-5}	−13.5	47.1
T_{69}	20.8	25.8	447.0	1.86×10^{-3}	−12.9	46.7
r5d	19.2	23.1	2241.3	13.29×10^{-3}	−14.2	38.1
d12	17.3	18.4	2066.1	32.55×10^{-3}	−17.6	44.2

[a] TFOs and DNA target as in Figure 1. [b] °C, estimated error in T_{max} ± 0.5°C. [c] M^{-1} s^{-1}. [d] s^{-1}. [e] kcal·mol^{-1}. [f] Estimated error ≤ 10%. [g] Estimated error ≤ 4%.

Thus, the simultaneous measurement of the absorption at 260 and 300 nm allows distinguishing between and characterizing these two transitions. Figure 2 shows melting profiles at 260 and 300 nm for the triplexes **d12:dh** (top) and **r12:dh** (bottom) as examples. Hysteresis can be observed in the region of the triplex transitions, where the kinetics of the process are not fast enough to reach equilibrium at the heating or cooling rate used (8.3×10^{-3} K/s).

Only at pH 5.9 were the T_m values of all triplexes within the required temperature window necessary for exact data acquisition. At this pH, all triplexes melt with a broad hysteresis in their melting curve. The kinetic data were therefore primarily determined at pH 5.9 as outlined in the materials and methods section. In brief, the kinetic constants k_{on} and k_{off} for each triplex were obtained according to eq 2a,b. The activation energies for the association and dissociation (E_{on} and E_{off}) were then determined from the slopes in plots of $\ln(c \cdot k_{on}/2)$ versus T^{-1} and $\ln(k_{off})$ versus T^{-1} resp (Figure 3). The thermodynamic melting temperature T_m, was determined from the intersection point of both plots for each TFO. All data are summarized in Table 1. Additional data for suitable TFO candidates at pH values different from 5.9 are contained in Table 2. We note here that the T_m represents a thermodynamic parameter, while the T_{max} has no specific thermodynamic relevance.

The stability of all triple helices studied decreased linearly and uniformly with the increase of the pH between 5.1 and 6.7, with a slope of ca. 26 °C/pH unit (Figure 4). This behavior was expected due to the need of cytosine protonation for triple-helix formation (*35*−*36*). The fact that destabilization was similar whether deoxyribo- or ribonucleotides was present in the TFOs is in agreement with the presumption that the pK_a of dC within an oligonucleotide is similar to that of rC (*37*), irrespective of the nature of the sugar unit of the nearest neighbor.

To check whether the differences in stability of triplexes investigated are related to differences in conformation, as proposed by other authors (*19*), we measured circular dichroism (CD) and electrophoretic mobility of the triplex components (single strands, double, and triple helices). CD spectra (Figure 5) were measured at low temperature to ensure the fully paired state of the triplexes. Compared to the double helix, a red shift of the positive band (260−300 nm) is observed in all cases, as well as the inversion of the signal at 220 nm. No relevant changes in the CD spectra of the different triplexes could be observed. The main difference that can be seen between the triplexes is the intensity of the positive band that is maximal for **T_{12}:dh** and minimal for **d12:dh**, with medium values in the other cases. In all cases the CD peak of the single-stranded TFOs at 260−300 nm

Table 2: Thermodynamic and Kinetic Data of Triple-Helix Formation as Determined from the Heating and Cooling Profiles of the UV-Melting Curves (See Materials and Methods Section) at pH Values Different from 5.9[a]

TFO	pH	T_m[b]	T_{max}[b]	k_{on}[c]	k_{off}[d]	E_{on}[e,f]	E_{off}[e,g]
r12	5.14	53.0	58.0	1.7×10^4	8.9×10^{-6}	−14.6	50.2
r11	5.15	50.7	55.6	6.8×10^3	$9.0 \cdot 10^{-6}$	−10.3	53.0
r11	6.71	7.4	12.3	1.08×10^2	0.188	−12.6	43.7
T12	6.71	10.4	14.0	1.73×10^2	9.84×10^{-2}	−13.8	41.4
T34	5.12	49.3	54.0	6.5×10^3	1.79×10^{-5}	−7.1	52.9
T34	6.70	5.2	7.0	1.49×10^2	0.814	−14.3	43.6
4T	5.15	50.7	54.5	8.6×10^3	2.79×10^{-5}	−10.2	44.0
4T	6.69	7.6	7.8	2.76×10^2	2.86	−20.2	50.0
dU6	5.16	51.2	52.6	1.58×10^4	2.61×10^{-6}	−9.6	71.0
T6	5.55	36.9	40.5	1.5×10^3	1.6×10^{-4}	−8.7	52.4
T6	6.29	14.2	20.0	2.27×10^2	4.7×10^{-2}	−11.0	47.9
T9	5.54	37.3	41.2	1.3×10^3	1.2×10^{-4}	−9.4	52.9
T9	6.30	15.2	19.9	2.50×10^2	3.18×10^{-2}	−10.3	46.1
T69	5.12	42.7	45.1	2.4×10^3	4.60×10^{-5}	−6.6	53.3
T69	6.31	10.3	13.7	1.63×10^2	0.199	−13.7	47.6
r5d	5.15	42.7	45.0	1.11×10^4	1.39×10^{-4}	−8.8	57.0
r5d	5.53	31.8	33.7	3.5×10^3	1.84×10^{-3}	−14.4	52.7
d12	5.54	27.3	28.5	5.3×10^3	1.32×10^{-2}	−9.1	61.0

[a] TFOs and DNA target as in Figure 1. [b] °C, estimated error in T_{max} ± 0.5°C. [c] M^{-1} s^{-1}. [d] s^{-1}. [e] kcal mol^{-1}. [f] Estimated error ≤ 10%. [g] Estimated error ≤ 4%.

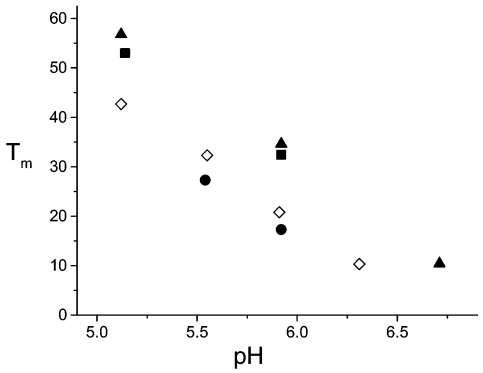

FIGURE 4: Thermodynamic T_m values of selected triple helices at various pH values. ■ **r12**, ● **d12**, ▲ **T_{12}**, and ◊ **T_{69}**.

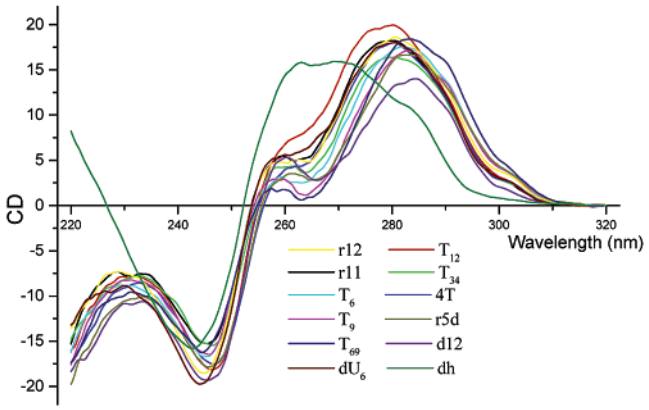

FIGURE 5: CD profiles (pH 5.9) of the hairpin duplex and the 12 triplexes with the TFOs depicted in Figure 1.

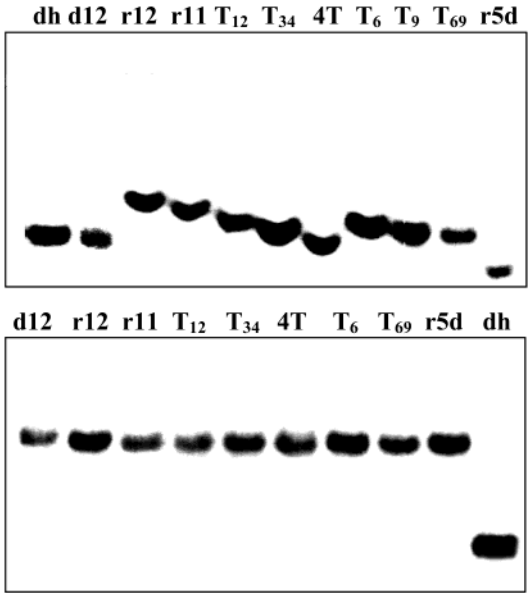

FIGURE 6: Nondenaturing polyacrylamide gel (4°C) showing the relative mobilities of the TFO single strands (top) and of the duplex and the corresponding triplexes (bottom).

clearly diminished between pH 5.0 and 6.0, as a consequence of cytosine deprotonation (results not shown). The relative similarity of the CD spectra prompted us to conclude that only little structural variation is present, indicating that the overall conformation of the triplexes are similar.

This conclusion is supported by the results of electrophoretic mobility measurements (Figure 6). Under nondenaturing conditions, the mobilities of TFO single strands are clearly different, depending on their nucleotide composition. By contrast, triple helices show similar mobility irrespective of the nature of the TFO. We interpret this result as an indication for the similarity of the triplex structures and the diversity of the single strand structures.

DISCUSSION

Sequence Composition Dependence of the T_m. The main differences between deoxyribo- and ribonucleotides are (i) the 2′-OH group, which has been shown to interact with neighboring strands and increase the stability of triple-helical structures (*16*), (ii) the 5-Me group of dT as compared to rU, which affects the stacking and solvation of the triple helix and which, as in the case of 5-Me-dC, was found to have positive (*38*−*39*) or neutral (*19*, *40*) effects on triplex stability, and (iii) the preferred conformation of the sugar ring (C3′-endo for ribo-, C2′-endo for deoxyribonucleosides). The conformation of DNA triple helices were extensively studied by NMR methods (*14*, *20*−*25*). These results showed that TFOs adopt mixed conformations, with dC^+ having a general preference for the C3′-endo form while dT having a preference for the C2′-endo form. One of the questions of our recent study (*32*) was whether TFOs composed of rC/dC and dT/rU nucleotides could lead to triple helices with increased stability, relative to pure ribo- or deoxyribo-TFOs.

We found that in the present sequence context, the RNA TFO **r12** forms a more stable triple helix than does the corresponding DNA TFO **d12**. The T_m of **r12:dh** is higher by some 15°C relative to that of **d12:dh**, at all pHs investigated (5.1−6.7). This is in agreement with previous results comparing R:D·D and D:D·D triple helices (*13*−*17*). With respect to the mixed backbone TFOs, the following behavior was observed. The substitution of all internal dC by rC (**d12** → **r5d**) gives a slight stabilization of the triple helix (0.4 °C/nucleotide), still far from the stability of **r12:dh** (Table 1). This result shows that, at least in this case, the use of a TFO with conformational backbone adaptability gives little thermodynamic advantage compared to an all-RNA TFO. The reason for this could be that the conformational inhomogeneity of the TFO has no energetic consequences on triplex stability, or that the interactions of the 2′-OH groups of the TFO within the triplex are more important for stability.

In the case of rU → dT substitutions, the stability changes depend largely on the position of the substitutions, allowing us to define three different environments in our system. First, rU → dT substitutions at the 5′-end of the TFO (**r11** → $\mathbf{T_{12}}$) thermally stabilize the triplex by some 3 °C. The unexpected result that $\mathbf{T_{12}}$, a mixed-backbone TFO, leads to a more stable triple helix than **r12** can be explained by a more favorable solvation due to the 5-Me groups of terminal thymines, or by a more efficient stacking of thymines at the end of the triple helix. Whatever the reason, it is clear that the replacement of deoxyribo- for ribosugar units at the 5'terminus of the TFO does not appreciably alter triple-helix stability. The second case is the substitution of rU at positions 3 and 4 for dT (**r11** → $\mathbf{T_{34}}$), which destabilizes the triple helix by some 2.5 °C. The destabilization is most probably due to the rC^+, neighboring $\mathbf{dT_4}$ in the sequence. The observation that the T_m of **4T:dh** is similar to that of **r11:dh**, due to the counterbalancing of the effects of $\mathbf{T_{12}}$ and $\mathbf{T_{34}}$, supports this view and also shows that a TFO with one-third of deoxyribonucleotides at well-chosen positions can be at least as stable as an all-RNA TFO.

The third case is the rU → dT substitution at positions 6 and/or 9 (**r11** → $\mathbf{T_6}$, $\mathbf{T_9}$ or $\mathbf{T_{69}}$; **4T** → **r5d**). Here a clear, additive destabilization of almost 6 °C is observed for each substitution, which is in contrast to the almost isoenergetic substitutions at the 5′-end. From this it becomes clear that the sequence plays a key role in the stability of partially modified triplexes. To probe an eventual role of the 5-Me group of thymine in this destabilizing effect, we synthesized the oligo $\mathbf{dU_6}$, where a deoxyuridine is introduced at position 6 (Figure 1). The stability of $\mathbf{dU_6}$**:dh** is between those of **r11:dh** and $\mathbf{T_6}$**:dh**. This means that the 5-Me group of the thymine at position 6 has a negative effect on the stability of the triple helix. This has never been described for other triple helices and is contrary to what has been found by other authors (*19*, *40*−*41*), and the reason is largely unknown.

Activation Energies. During the nucleation-zipping process of triple-helix formation, the activation energy E_{on} depends on the number of base triplets that are necessary to form the nucleus that will then rapidly evolve to the complete triple helix. In our experiments, the E_{on} values for all TFOs studied were between −7 and −20 kcal mol^{-1}. These values are in agreement with those published earlier at pH 6.8 (*28*). E_{on} shows a slight but measurable increase that goes parallel with the increase in the pH between 5.1 and 6.7. At lower pH, cytosines in the TFO are protonated to a greater extent, lowering the electrostatic repulsion between the TFO and the double helix, and thus favoring the association process. In addition, the different conformational preferences of

neutral and protonated cytidines can also play a role. The accuracy of the E_{on} calculations (see Table 1) forbids us to take further conclusions based on these results. The activation energy for the dissociation (E_{off}) could be calculated with higher accuracy, and also in this case, very similar values were found at all pHs and with all TFOs. The obtained values, between 38 and 61 kcal mol^{-1}, are also in this case in good agreement with those previously reported (*28*). A little decrease of E_{off} with the increase of the pH was observed. The diverging variations in E_{on} and E_{off} give homogeneous $\Delta H°$ values ($\Delta H° = E_{on} - E_{off}$).

Rate Constants. The values obtained for k_{on} and k_{off} are similar to previously reported data on R:D·D and D:D·D triple-helix formation (*19*, *41*−*43*). The T_m of the triple helices were obtained from the intersection points of the plot of $\ln(c \cdot k_{on}/2)$ and $\ln(k_{off})$ as a function of $1/T$, using eq 4a,b. The convenience of the use of the nucleation-zipping model for the triplex−duplex transition is demonstrated by the linearity of the plots (Figure 3a,b). As discussed above, the values of the activation energies obtained from the slope of these graphs stay within a narrow range at all pHs and for all TFOs studied.

Focusing on **r12:dh** and **d12:dh** (the R:D·D and D:D·D triplexes, respectively) at pH 5.9, we find that both k_{on} and k_{off} are faster in the case of the all-DNA triplex. Nevertheless, the differences are of only a factor of 2 for k_{on}, in contrast to a factor of 500 for k_{off}. From this we conclude that the difference in triplex stability is driven by the differences in the dissociation rate. A big difference in k_{off} has a dramatic consequence on the lifetime of the corresponding triplex. This lifetime is of about 1 h for **r12:dh**, and only some 9 s for **d12:dh**, at 30°C and pH 5.9. Thus, when melting profiles are recorded at too high heating rates so that equilibrium conditions are not fulfilled, the difference in T_{max} between a R:D·D and a D:D·D triple helix will overestimate the true T_m difference. In our case, nonequilibrium T_{max} values differ by 19.3 °C at pH 5.9, compared to 15.1 °C for the true thermodynamic T_m values (Table 1). At the same time, van't Hoff enthalpies, extracted from nonequilibrium heating curves by curve-fitting procedures, will be larger than the true ones, especially in the case of slow kinetics, e.g., for **r12:dh**. This again overestimates the differences between the stability of both types of triple helices. These considerations can explain, at least in part, why larger differences in stability between similar R:D·D and D:D·D triple helices are found when melting experiments are used instead of calorimetric methods (*13*−*19*).

For the mixed backbone TFOs, very different kinetic behaviors are observed, depending on the position and nature of the substitutions. **r5d:dh**, together with **d12:dh**, show a higher k_{off} than any other triplex. This indicates that the 5-Me group of thymine plays a key role in the dissociation kinetics of the TFOs, due to its effect on solvation and stacking and/or the steric hindrance that it may exert within the triplex. The k_{on} values are also among the faster ones at pH 5.9. The difference decreases at lower pH. Nucleation can occur at any point of the TFO, but we can suppose that cytosine-rich regions are favored at low pH because of the positive charge that they carry, while other factors (local conformation, solvation, 2′-OH interactions) become more important at higher pH values. With this in mind, we can attempt to explain the association behavior of **r5d** by a favorable effect of dT over rU, which is softened at lower pH by the more important participation of the protonated cytosines in the nucleation step.

Looking at **4T:dh** and **T_{69}:dh** and taking **r5d:dh** and **r11:dh** as references, it clearly appears at pH 5.9 that the dT track at the 5′-end contributes solely to speeding up the association process. The same substitutions at positions 6 and 9 have little effect on the association but greatly contribute to a faster k_{off}. At lower pH, where protonated cytosines preferentially participate in the nucleation step, the effect of the 5′-dT track on k_{on} is overcome, while the negative effect of dT_6 and dT_9, which are now in the region where nucleation takes place, is increased. **T_6:dh** and **T_9:dh** show, as expected, similar but weaker effects on k_{on} and k_{off} relative to **T_{69}:dh**. Their effect on k_{on} at pH 5.1 is negligible, for the same reasons as that in the case of **4T:dh**.

The study of **T_{12}:dh** and **T_{34}:dh** allows to take a closer look into the kinetic effects of the 5′-dT tract. dT_1 and dT_2 mainly contribute to the increase of k_{on} observed in **4T:dh** when compared to **r11:dh**, while dT_3 and dT_4 are the only involved in the increase of k_{off}, probably because of the vicinity of ribocytidines. These two effects together explain the high thermodynamic stability of **T_{12}:dh**.

Finally, the stabilizing effect of dU6 (in **dU:dh**) as compared to dT (in **T_6:dh**) is translated, in terms of kinetics, to a little but favorable effect in both k_{on} and k_{off}. It means that the presence of a 2′-H and/or a 5-Me groups at the nucleotide in this position has very similar kinetic consequences, mainly a net increase of the k_{off} of the triplex.

CONCLUSIONS

The use of TFOs as tools in molecular biology or in therapy requires a deeper understanding of the mechanism of formation and the kinetic properties of the triple helices. For example, TFOs with slow dissociation kinetics should be preferred in the antigene strategy for blocking gene expression, as they will stay longer on the target sequence, thus interfering with replication or translation. For the use as artificial nucleases (when a functional unit is attached to the TFO that catalyzes the cleavage of the target after triplex formation), fast kinetics that make the TFO rapidly available for hybridization with a new target should be preferred. Our results demonstrate that the stability and especially the kinetics of triple-helix formation can be varied and fine tuned by doping ribooligonucleotide-TFOs with deoxyribonucleotides. Not only the nature or the number of such substitutions, but their position within the sequence is also important. It is conceivable that out of the large body of existing nucleotide analogues, more structures will emerge that alter the association/dissociation kinetics of TFOs in a well-defined way. Detailed knowledge of the structural and mechanistic factors determining the binding kinetics is therefore a necessary prerequisite for advanced TFO design.

REFERENCES

1. Hecht, S. M., Ed. (1996) *Bioorganic Chemistry*: *Nucleic Acids*, Oxford University Press, New York.
2. Felsenfeld, G., and Rich, A. (1957) *Biochim. Biophys. Acta 26*, 457−468.
3. Felsenfeld, G., Davis, D. R., and Rich, A. (1957) *J. Am. Chem. Soc. 79*, 2023−2024.

4. Riley, M., Maling, B., and Chamberlin, M. J. (1966) *J. Mol. Biol. 20*, 359−389.
5. Morgan, A. R., and Wells, R. D. (1968) *J. Mol. Biol. 37*, 63−80.
6. Mirkin, S. M., Lyamichev, V. I., Drushlyak, K. N., Dobrynin, V. M., Filippov, S. A., and Frank-Kamenetskii, M. D. (1987) *Nature 330*, 495−497.
7. LeDoan, T., Perrouault, L., Praseuth, D., Habhoub, N., Decout, J. L., Thuong, N. T., Lhomme, J., and Hélène, C. (1987) *Nucleic Acids Res. 15*, 7749−7761.
8. Moser, H. E., and Dervan, P. B. (1987) *Science 238*, 645−650.
9. Radhakrishnan, I., and Patel, D. J. (1994) *Biochemistry 33*, 11405−11416.
10. Sun, J. S., and Hélène, C. (1993) *Curr. Opin. Struct. Biol. 3*, 345−356.
11. Vasquez, K. M., and Wilson, J. H. (1998) *Trends Biochem. Sci. 23*, 4−9.
12. Thuong, N. T., and Hélène, C. (1993) *Angew. Chem., Int. Ed. Engl. 32*, 666−690.
13. Roberts, R. W., and Crothers, D. M. (1992) *Science 258*, 1463−1465.
14. Asensio, J. L., Carr, R., Brown, T., and Lane A, N. (1999) *J. Am. Chem. Soc. 121*, 11063−11070.
15. Shimizu, M., Konishi, A., Shimada, Y., Inoue, H., and Ohtsuka, E. (1992) *FEBS Lett. 302*, 155−158.
16. Escudé, C., François, J. C., Sun, J. S., Ott, G., Sprinzl, M., Garestier, T., and Hélène, C. (1993) *Nucleic Acids Res. 21*, 5547−5553.
17. Noronha, A., and Damha, M. (1998) *Nucleic Acids Res. 26*, 2665−2671.
18. Han, H., and Dervan, P. B. (1993) *Proc. Natl. Acad. Sci. U.S.A. 90*, 3806−3810.
19. Torigoe, H., Shimizume, R., Sarai, A., and Shindo, H. (1999) *Biochemistry 38*, 14653−14659.
20. Liquier, J., Coffinier, P., Firon, M., and Taillander, E. J. (1991) *Biomol. Struct. Dyn. 9*, 437−445.
21. Macaya, R. F., Schultze, P., and Feigon, J. (1992*) J. Am. Chem. Soc. 114*, 781−783.
22. Liquier, J., Taillander, E., Klinck, R., Guittet, E., Gouyette, C., and Huynh-Dinh, T. (1995) *Nucleic Acids Res. 23*, 1722−1728.
23. Bartley, J. P., Brown, T., and Lane, A. N. (1997) *Biochemistry 36*, 14502−14511.
24. Tarköy, M., Phipps, A. K., Schultze, P., and Feigon, J. (1998) *Biochemistry 37*, 5810−5819.
25. Gotfredsen, C. H., Schultze, P., and Feigon J. (1998) *J. Am. Chem. Soc. 120*, 4281−4289.
26. Porschke, D., and Eigen, M. (1971) *J. Mol. Biol. 62*, 361−381.
27. Xodo, L. E., Pirully, D., and Quadrifoglio, F. (1997) *Eur. J. Biochem. 248*, 424−432.
28. Rougée, M., Faucon, B., Barcelo, F., Giovannangeli, T., Garestier, T., and Hélène, C. (1992) *Biochemistry 31*, 9269−9278.
29. Hildbrand, S., Blaser, A., Parel, S. P., and Leumann C. J. (1997) *J. Am. Chem. Soc. 119*, 5499−5511.
30. Imanishi, T., and Obika, S. J. (1999) *Synth. Org. Chem. Jpn. 57*, 77−88.
31. Prakash, T. P., Manoharan, M., Fraser, A. S., Kawasaki, A. M., Lesnik, E. A., and Owens, S. R. (2000) *Tetrahedron Lett. 41*, 4855−4859.
32. Bernal-Méndez, E., and Leumann, C. J. (2001) *J. Biol. Chem. 276*, 3532−3537.
33. Puglisi, J. D., and Tinoco, I. Jr. (1989) *Methods Enzymol. 180*, 304−325.
34. Lavelle, L., and Fresco, J. R. (1995) *Nucleic Acids Res. 23*, 2692−2705.
35. Asensio, J. L., Lane, A. N., Dhesi, J., Bergquist, S., and Brown, T. (1998) *J. Mol. Biol. 27*5, 811−822.
36. Plum, G. E., Park, Y. W., Singleton, S. F., Dervan, P. B., and Breslauer, K. J. (1990)*Proc. Natl. Acad. Sci. U.S.A. 87*, 9436−9440.
37. Lacroix, L., Mergny, J.-L., Leroy, J.-L., and Hélène, C. (1996) *Biochemistry 35*, 8715−8722.
38. Leitner, D., Schröder, W., and Weisz, K. (2000) *Biochemistry 39*, 5886−5892.
39. Bolton, P. H., and Kearns, D. R. (1979) *J. Am. Chem. Soc. 101*, 479−484.
40. Povsic, T. J., and Dervan, P. B. (1989) *J. Am. Chem. Soc. 111*, 3059−3061.
41. Torigoe, H. (2001) *Biochemistry 40*, 1063−1069.
42. Sugimoto, N., Wu, P., Hara, H., and Kawamoto, Y. (2001) *Biochemistry 40*, 9396−9405.
43. Bates, P. J., Dosanjh, H. S., Kumar, S., Jenkins, T. C., Laughton, C. A., and Neidle, S. (1995) *Nucleic Acids Res. 23*, 3627−3632.

BI025937M